Indian cratonic mantle beneath northern Qiangtang in eastern Tibet 11 Myr ago

Jun Wang[1†], Chuan-Bing Xu[1†, 2], Qiang Wang[1*, 2], Chris J. Hawkesworth[3*], Yi-Gang Xu[1, 2], Gong-Jian Tang[1], Derek Wyman[4], Andrew C. Kerr[5], Bing-Zhang Wang[6], Jin-Heng Liu[1], Wu-Fu Li[6], Shan-Ping Li[6], Yue Qi[1], Jie Li[1], Zhuo Xiao[7], Chun-Tao Wang[6]

†co-first authors; *Email: wqiang@gig.ac.cn, C.J.Hawkesworth@bristol.ac.uk

[1]State Key Laboratory of Deep Earth Processes and Resources, Guangzhou Institute of Geochemistry, Chinese Academy of Sciences, Guangzhou, 510640, China

[2]College of Earth and Planetary Sciences, University of Chinese Academy of Sciences, Beijing 100049, China

[3]School of Earth Sciences, University of Bristol, Wills Memorial Building, Queens Road, Bristol BS8 1RJ, UK

[4]School of Geosciences, The University of Sydney, NSW 2006, Australia

[5]School of Earth and Environmental Sciences, Cardiff University, Cardiff, CF10 3AT, UK

[6]Qinghai Geological Survey Institute, Xining, Qinghai 810012, China

[7]College of Artificial Intelligence, Guangxi Minzu University, Nanning, Guangxi, 530006, China

ABSTRACT

Establishing the northern limit of Indian lithosphere under the Tibetan Plateau is key to understanding India–Asia convergence mechanisms. Its location is disputed due to conflicting seismic interpretations, and in particular the inability to distinguish between the subducted Indian and thickened Tibetan lithospheres in tomographic images. We report the results of a new approach based on the petrology and geochemistry of Miocene (~11 Myr ago) lamproites recently discovered in northern Qiangtang of the Himalayan-Tibetan orogen. They are clearly distinguished from other orogenic lamproites by lead isotope ratios plotting to the left of the geochron, and their Pb-Nd-Os isotopes indicate an Archean (>2.7 Ga) Indian cratonic mantle source. This is compelling evidence that Indian cratonic mantle underthrust northward for ~600 km and had reached below northern Qiangtang in eastern Tibet at least 11 Myr ago. Such large-scale underthrusting of buoyant cratonic lithosphere resolves competing geophysical interpretations and plays an important role in shaping intraplate topography.

INTRODUCTION

Cenozoic convergence between the Indian and Asian plates created the Tibetan Plateau (Yin and Harrison, 2000). Models of convergence include subducting or underthrusting of the Indian lithosphere beneath Tibet (Argand, 1924), shortening and thickening of weak Tibetan lithosphere (Dewey et al., 1988), and eastward lateral extrusion of Tibet (Tapponnier et al., 2001). In principle, if crustal shortening and extrusion had absorbed all the convergence, there is no need for subduction of Indian lithosphere. However, the amount of Cenozoic shortening of Asian crust is poorly constrained, so it is disputed how much subduction of Indian lithosphere occurred beneath

Tibet (Johnson, 2002).

Geophysical images have led to contradictory interpretations of the surface position of the leading edge of Indian lithosphere. To the east of 90°E, some tomographic models show the high-velocity body, interpreted as the Indian lithosphere, does not extend beyond the Indus–Yarlung Zangbo suture (Fig. 1e–f; Hosseini et al., 2020; Li et al., 2008), while others suggest it is near the Bangong–Nujiang suture (Tilmann et al., 2003) or even extends beyond the Jinshajiang suture (Fig. 1a–d; Chen et al., 2017; Li and Song, 2018). For example, the underthrust Indian lithosphere in the UU-P07 model (Fig. 1a–c; Amaru, 2007) protrudes from the Main Frontal Thrust over 400–800 km (van Hinsbergen, 2022) and is separated from the surrounding Yangtze and Tarim cratons by two large low-velocity bodies.

Discrepancies between the different tomographic images may result from sparse distribution of seismic stations in Tibet, different seismic phases and algorithms used in the inversion, and the inability to distinguish between the subducted Indian and thickened Tibetan lithospheres (Chen et al., 2017). Geophysical research also cannot readily constrain the timing of Indian lithosphere reaching its current position beneath Tibet. An alternative approach is to interrogate the magmatic record and to establish the age and northern extent of magmatic rocks that contain contributions from the Indian plate.

RESULTS

The Tibetan Plateau consists of the Kunlun–Qaidam–Qilian, Songpan–Ganzi, Qiangtang, Lhasa and Himalaya terranes (Fig. 1a). The Indian continent has five cratons that are Archean in age (Yin and Harrison, 2000). The Qiangtang Terrane can be subdivided into the Southern and

Northern Qiangtang terranes (NQT) by the Longmuco–Shuanghu suture (Zhang et al., 2016). Eocene-Oligocene mafic to felsic magmatic rocks and Pliocene-Quaternary felsic lavas occur in the central (west of 92°E) and eastern (i.e., Yushu area) parts of the NQT (Wang et al., 2016), and we report new results on the recently discovered late Miocene ultrapotassic lavas in the Yushu area. The samples are from three locations < 7 km apart (Fig. S1), and are classified into low-, medium-, and high-Si lavas. Phlogopite $^{40}Ar/^{39}Ar$ plateau ages (Fig. S2) indicate that the Yushu low- (10.7 ± 0.1 Ma), medium- (11.0 ± 0.1 Ma), and high-Si (10.8 ± 0.1 Ma) lavas are broadly contemporaneous (~ 11 Ma).

The Yushu low-Si lavas fit the geochemical and mineralogical criteria of lamproites (Mitchell and Bergman, 1991) , they are ultrapotassic (K_2O/Na_2O = 2.6–9.5) with low CaO (< 9.6 wt% on a volatile-free basis) and FeO (< 7.0 wt%) and high Mg# (molar 100×Mg/[Mg + Fe] > 72) and Ba (5436–20187 ppm; Table S1); they contain typomorphic minerals of K-rich richterite, Ti-rich and Al-poor phlogopite, Fe-rich leucite, and forsteritic olivine (Table S2–5 and Fig. S3–4). In contrast, the medium- and high-Si lavas contain sanidine instead of richterite, leucite and olivine (Fig. S3–4). The Yushu lavas show marked increases in $^{206}Pb/^{204}Pb_i$ (16.645 to 18.258), $^{207}Pb/^{204}Pb_i$ (15.573 to 15.764), $^{187}Os/^{188}Os_i$ (0.169 to 0.641) and $\varepsilon_{Nd}(t)$ (-20.4 to -12.5) with increasing SiO_2 (51.4 to 57.5 wt%) and decreasing Mg# (75 to 66) and Os (240 to 37 ppt) (Fig. 2). *In situ* analysis of Pb isotopes in fresh feldspar (Fig. S3) and Nd isotopes in clinopyroxene record similar trends to those of their whole-rock hosts (Fig. 2c–d).

DISCUSSION

Assimilation of Basement Rocks

Increasing $^{206}Pb/^{204}Pb_i$ and $\varepsilon_{Nd}(t)$ in the Yushu lavas with increasing SiO_2 and decreasing Mg# indicates the effects of assimilation and fractional crystallization (AFC) processes. AFC, rather than bulk mixing, reproduces the observed Os isotopic variations, as bulk mixing would require an unreasonably large amount of crustal material to be incorporated into the high-Mg# (>72) and Os (136–240 ppt) lamproites (Fig. 2b). Sub-rounded green clinopyroxenes occur in the cores or mantles of a few clinopyroxene phenocrysts in the Yushu lamproites, and they have significantly lower Mg# (< 63) and higher $\varepsilon_{Nd}(t)$ values than their colorless rims (Mg# > 90; Fig. 2d and Fig. S5). This suggests that green clinopyroxenes crystallized from felsic melts produced by melting of relatively young crustal sources. Green-core clinopyroxenes commonly have high jadeitic components, indicating high-pressure crystallization (Dobosi and Fodor, 1992). The clinopyroxene barometers yield crystallization depths of 40–60 km (see Fig. S7 and the Supplemental Material).

Considering that the NQT reached its current elevation in the Eocene (Ding et al., 2022), the present day and Miocene crust thickness (60–65 km; Xia et al., 2023) are similar. Assimilation is thermally coupled to crystallization, as evidenced by Os isotopes. The lower-crustal crystallization depths indicate that the contaminant is Yushu basement rocks, and that they have higher Nd and Pb isotopes than the high-Si lavas ($\varepsilon_{Nd}[0] > -12.6$; $^{206}Pb/^{204}Pb > 18.264$), and that the lamproites evolved into high-silica lavas by AFC. This is consistent with the isotope ratios of the granulite xenoliths ($\varepsilon_{Nd}[0] = -4.7$ to -11.4; $^{206}Pb/^{204}Pb = 18.68$ to 19.19; Fig. 2a and 3b) entrained in the Cenozoic felsic lavas of central NQT, and it highlights that neither the central nor the eastern NQT basement displays the highly unradiogenic Pb and Nd isotopic ratios of Archaean cratonic granulites (Fig. 2a). The distinctive least radiogenic Nd and Pb isotopic ratios in the Yushu lamproites are taken to characterize their mantle sources, since the lamproites are primitive in composition, and relatively little affected by AFC reflected in the more evolved lithologies.

Archean Indian Cratonic Mantle Source

Cenozoic lamproites worldwide occur in both cratonic (or anorogenic) and Tethyan orogenic settings, but they have strikingly different Pb isotope ratios that plot to the left and right of the 4.56 Ga geochron, respectively (Tommasini et al., 2011; Fig. 2a). The cratonic and orogenic lamproites both originate from lithospheric mantle, but the enrichment was at least Mesoproterozoic in age for the cratonic lamproites, and relatively recent for the orogenic lamproites (Mitchell and Bergman, 1991). The high $^{187}Os/^{188}Os$ ratios (>0.13) for high-Os (>100 ppt) ultrapotassic rocks (including lamproites; Fig. 2b) worldwide suggest derivation from lithospheric mantle consisting of phlogopite-bearing pyroxenitic veins and ambient peridotites (Foley, 1992; Prelević et al., 2015). The markedly low $^{206}Pb/^{204}Pb$ and ε_{Nd} of Yushu lamproites relative to oceanic basalts argue against an origin within the convecting asthenosphere or a mantle plume (Fig. 2a; Davies et al., 2006).

Most of Earth's accessible rocks plot significantly to the right of the 4.56 Ga geochron (Doucet et al., 2023; Fig. 2a), and only rare lamproites or alkalic basalts (Fraser et al., 1985) and lower-crustal granulites (Rudnick and Goldstein, 1990) from Archean cratons plot significantly to the left of the geochron. This is because cratons have not experienced tectono-magmatic disturbance for >1 Gyr, and areas of low $^{238}U/^{204}Pb$ (μ) values have had sufficient time to develop low time-integrated Pb isotopes ratios. The Yushu lamproites are similar to cratonic lamproites in that their Pb isotopes plot significantly to the left of the geochron (Fig. 2a). The highly unradiogenic component in their mantle sources, here referred to as the Yushu component, was either derived from ancient cratonic mantle or conceivably from young orogenic mantle recently enriched by ancient granulite-derived melts. However, ancient cratonic granulites are strongly depleted in heat-producing elements (e.g., K) and H_2O (Rudnick and Goldstein, 1990; Bolhar et al., 2007), making them unlikely to serve as metasomatic agents in the mantle source of K- and H_2O-rich lamproites (Mitchell and Bergman, 1991).

We used a three-stage Pb growth model, including a Monte Carlo refinement procedure, to evaluate combinations of μ and age (T) in the evolution of the Yushu component. The three stages are distinguished by subscripts 1, 2, and 3 for T and μ (Fig. 3a). The definitions and interdependencies of all parameters (Fig. S6) are described in the Supplemental Material. A total of 1×10^{10} calculations were performed. The 125,126 successful combinations in Fig. 3a were obtained by limiting the range of μ_2 ($>\mu_1$) to values reasonable for the crust, considering that the crust is more radiogenic in Pb isotopes than the Bulk Silicate Earth (Doucet et al., 2023). The calculated results indicate that both T_2 and T_3 exceed 2.7 Ga. Furthermore, the chondritic uniform reservoir (CHUR) Nd model ages (T_{CHUR} = 2.9 Ga; Table S7) can be regarded as an estimate of the minimum period required for a source with the sample Sm/Nd to evolve the lowest ε_{Nd} values observed in the Yushu lamproites from CHUR. This is because T_{CHUR} values are positively correlated with the assumed source Sm/Nd, which is expected to be higher than the sample Sm/Nd. Thus, the Yushu component appears to have maintained a closed system in cratonic mantle for at least 2.7 Gyr.

The presence of this Archean Yushu component requires that either the NQT includes cratonic lithosphere with Archaean basement rocks, or the Yushu component was derived from Indian cratonic mantle subducted during the ongoing India–Asia convergence. The relatively radiogenic Pb isotope ratios of basement rocks indicated by both the Yushu high-Si lavas from eastern NQT and the granulite xenoliths from central NQT resemble those of the granulite xenoliths from Phanerozoic orogenies, and they are very different isotopically from granulites from cratons (Fig. 2a). Thus, the NQT lacks the Archean basement rocks that are unique to cratons, and our compiled isotopic data of Mesozoic-Cenozoic rocks (n = 1134) indicates that the pre-Miocene Qiangtang lithosphere was characterized by relatively radiogenic Pb and Nd isotope ratios with no evidence for ancient components with unradiogenic Pb isotopes, or $\varepsilon_{Nd}(0)$ values as low as -20 (Fig. 2a and 3b). The Yushu Eocene (35–40 Ma) potassic mafic lavas have more radiogenic Nd and Pb isotopes than the Yushu Miocene (11 Ma) lamproites (Fig. 3b), indicating that the Indian craton reached below the Yushu area between ~35 and 11 Ma.

The northward underthrusting of Indian slab triggered delamination of the Tibetan lithosphere and asthenospheric upwelling at its edge (Kelly et al., 2020), and the interior of the Indian slab may be penetrated by asthenospheric upwelling due to localized tearing (Fig. 4; Hou et al., 2023). These upwellings induced lithospheric melting that generated ≤11 Ma ultrapotassic magmas in Lhasa and Qiangtang (Fig. 1a). Tethyan orogenic lamproites exhibit high Th/La ratios (0.88 ± 0.47, 1σ), characteristic of the Lhasa lamproites (1.38 ± 0.38) but distinct from cratonic (0.12 ± 0.04) and Yushu (0.22 ± 0.01) lamproites (Tommasini et al., 2011). This high Th/La (>0.5) signature suggests contributions from the lawsonite in young, shallow, blueschist-bearing lithosphere (Wang et al., 2021). The restriction of these blueschists and high-Th/La potassic lavas to the Phanerozoic (Wang et al., 2021) implies Precambrian mantle enrichment for the Yushu lamproite sources. In contrast, the Lhasa mafic rocks show decreasing $\varepsilon_{Nd}(0)$ values since the initial India–Asia collision (Fig. 3b), suggesting that their mantle sources were enriched by the

Cenozoic subduction of the Indian crust (Fig. 4; Guo et al., 2015).

Implications

The northern limit of the Indian lithosphere, as interpreted by different geophysical studies, vary most significantly in eastern Tibet (Fig. 1). Our samples highlight that in eastern Tibet the underthrust Indian cratonic mantle reached below NQT at least ~11 Ma and northward from the Main Frontal Thrust over ~600 km in the direction of GPS motion (Fig. 1a). This is consistent with the tomographic models of Fig. 1a–d and thermal-lithosphere thickness (Xia et al., 2023), in which a thick (> 200 km) high-velocity body below the eastern NQT continues southward into the Indian craton. Therefore, the large low-velocity anomalies in the upper mantle beneath our study area, as shown in the tomographic models of Fig. 1e–f, arguably merit some re-evaluation.

Some tomographic models show thick (>200 km) high-velocity bodies beneath Tibet (Fig. 1a–d). One interpretation is that they are the result of the thickening of the normal thickness Tibetan lithosphere through pure shear shortening, rather than reflecting underthrust Indian lithosphere (Molnar et al., 1993; McKenzie and Priestley, 2016). This perspective reflects classical plate tectonics theory, which holds that continental lithosphere, relative to oceanic lithosphere, is buoyant and typically resists subduction at collisional boundaries. However, the case presented here provides compelling evidence that continental lithosphere, even of a buoyant craton, can underthrust significant distances from the collisional boundary.

The eastern, southern, and western regions (Figs. 1a and 4) of Tibet are characterized by thick thermal lithosphere and low surface heat flow (Xia et al., 2023), which may have been reduced by underthrust Indian lithosphere. The topographic relief in these regions is more pronounced compared to the relatively flat central–northern part with a thinner lithosphere (Fig. 1a and Fig. S8). The flat topography may reflect a combination of high heat flow, crustal melting, rheological weakening, and induced crustal flow (Fig. 4; Spencer et al., 2021; Wang et al., 2016). Large-scale northward underthrusting of the Indian lithosphere explains the intraplate deformation and associated uplift observed in the northern Tibetan Plateau and the Central Asian region since ~11 Ma (Fig. S9).

ACKNOWLEDGEMENTS

We acknowledge editor Marc Norman, Sukanta Dey, and other anonymous reviewers for constructive comments, and S.H. Zou, Y.W. Wei and Z. Zhang for discussion. This study was supported by the National Natural Science Foundation of China (42021002 and 42472073) and the Second Tibetan Plateau Scientific Expedition and Research (2019QZKK0702). This is contribution no. IS-XXXX from GIGCAS.

FIGURE CAPTIONS

Fig. 1. (a) Depth slice at 110 km below India and Tibet from the P-wave UU-P07 model (Amaru, 2007). The yellow line is interpreted as the northern margin of underthrust Indian continent below Tibet (van Hinsbergen, 2022). The regions in Tibet with thermal-lithosphere thickness of >200 km are from Xia et al. (2023). (b–f) Vertical-cross sections along two profiles in (a) derived from the UU-P07 (Amaru, 2007), FWEA23 (Liu et al., 2024), DETOX-P3 (Hosseini et al., 2020) and MITP08 (Li et al., 2008) models. The GPS movement direction and velocity are from Wang et al. (2001).

Fig. 2. Pb-Os-Nd isotopes of Yushu ultrapotassic rocks. The data sources in (a–b) and assimilation and fractional crystallization (AFC) and mixing parameters in (b) are given in the Supplemental Material. Mixing and AFC1-2 curves are marked in 10% and 1% increments, respectively. The error bars for mineral symbols are 1 standard error.

Fig. 3. (a) Results of Monte Carlo modeling showing interdependence between T_2, T_3 and μ_2 (see the inset and Supplemental Material for definitions of T and μ). (b) Variations of $\varepsilon_{Nd}(0)$ and $^{206}Pb/^{204}Pb$ (measured values) in the Mesozoic–Cenozoic rocks in Qiangtang and Lhasa over time. Data sources in (b) are provided in the Supplemental Material.

Fig. 4. Idealized cartoon depicting the underthrusting and tearing of Indian craton, delamination of Tibetan lithospheric mantle, and associated Miocene-Quaternary magmatism.

REFERENCES

Amaru, M., 2007, Global travel time tomography with 3-D reference models, Utrecht University.

Argand, E., 1924, La tectonique de l'Asie.: International Geological Congress Report of Sessions, v. 13, p. 171-372.

Bolhar, R., Kamber, B. S., and Collerson, K. D., 2007, U-Th-Pb fractionation in Archaean lower continental crust: Implications for terrestrial Pb isotope systematics: Earth and Planetary Science Letters, v. 254, no. 1-2, p. 127-145.

Chen, M., Niu, F. L., Tromp, J., Lenardic, A., Lee, C. T. A., Cao, W. R., and Ribeiro, J., 2017, Lithospheric foundering and underthrusting imaged beneath Tibet: Nature Communications, v. 8, p. 15659.

Davies, G. R., Stolz, A. J., Mahotkin, I. L., Nowell, G. M., and Pearson, D. G., 2006, Trace element and Sr-Pb-Nd-Hf isotope evidence for ancient, fluid-dominated enrichment of the source of Aldan shield lamproites: Journal of Petrology, v. 47, no. 6, p. 1119-1146.

Dewey, J. F., Shackleton, R. M., Chang, C. F., and Sun, Y. Y., 1988, The Tectonic Evolution of the Tibetan Plateau: Philosophical Transactions of the Royal Society a-Mathematical Physical and Engineering Sciences, v. 327, no. 1594, p. 379-413.

Ding, L., Kapp, P., Cai, F. L., Garzione, C. N., Xiong, Z. Y., Wang, H. Q., and Wang, C., 2022, Timing and mechanisms of Tibetan Plateau uplift: Nature Reviews Earth & Environment, v. 3, no. 10, p. 652-667.

Dobosi, G., and Fodor, R. V., 1992, Magma Fractionation, Replenishment, and Mixing as Inferred from Green-Core Clinopyroxenes in Pliocene Basanite, Southern Slovakia: Lithos, v. 28, no. 2, p. 133-150.

Doucet, L. S., Li, Z. X., Fougerouse, D., Olierook, H. K. H., Gamaleldien, H., Kirkland, C. L., and Hartnady, M. I. H., 2023, The global lead isotope system: Toward a new framework reflecting Earth's dynamic evolution: Earth-Science Reviews, v. 243, p. 104483.

Foley, S., 1992, Vein-Plus-Wall-Rock Melting Mechanisms in the Lithosphere and the Origin of Potassic Alkaline Magmas: Lithos, v. 28, no. 3-6, p. 435-453.

Fraser, K. J., Hawkesworth, C. J., Erlank, A. J., Mitchell, R. H., and Scott-Smith, B. H., 1985, Sr, Nd and Pb isotope and minor element geochemistry of lamproites and kimberlites: Earth and Planetary Science Letters, v. 76, no. 1, p. 57-70.

Guo, Z. F., Wilson, M., Zhang, M. L., Cheng, Z. H., and Zhang, L. H., 2015, Post-collisional Ultrapotassic Mafic Magmatism in South Tibet: Products of Partial Melting of Pyroxenite in the Mantle Wedge Induced by Roll-back and Delamination of the Subducted Indian Continental Lithosphere Slab: Journal of Petrology, v. 56, no. 7, p. 1365-1405.

Hosseini, K., Sigloch, K., Tsekhmistrenko, M., Zaheri, A., Nissen-Meyer, T., and Igel, H., 2020, Global mantle structure from multifrequency tomography using P, PP and P-diffracted waves: Geophysical Journal International, v. 220, no. 1, p. 96-141.

Hou, Z. Q., Wang, R., Zhang, H. J., Zheng, Y. C., Jin, S., Thybo, H., Weinberg, R. F., Xu, B., Yang, Z. M., Hao, A. W., Gao, L., and Zhang, L. T., 2023, Formation of giant copper deposits in Tibet driven by tearing of the subducted Indian plate: Earth-Science Reviews, v. 243, p. 104482.

Johnson, M. R. W., 2002, Shortening budgets and the role of continental subduction during the India-Asia collision: Earth-Science Reviews, v. 59, no. 1-4, p. 101-123.

Kelly, S., Beaumont, C., and Butler, J. P., 2020, Inherited terrane properties explain enigmatic post-collisional Himalayan-Tibetan evolution: Geology, v. 48, no. 1, p. 8-14.

Li, C., Van der Hilst, R. D., Meltzer, A. S., and Engdahl, E. R., 2008, Subduction of the Indian lithosphere beneath the Tibetan Plateau and Burma: Earth and Planetary Science Letters, v. 274, no. 1-2, p. 157-168.

Li, J. T., and Song, X. D., 2018, Tearing of Indian mantle lithosphere from high-resolution seismic images and its implications for lithosphere coupling in southern Tibet: Proceedings of the National Academy of Sciences of the United States of America, v. 115, no. 33, p. 8296-8300.

Liu, C., Banerjee, R., Grand, S. P., Sandvol, E., Mitra, S., Liang, X., and Wei, S., 2024, A high-resolution seismic velocity model for East Asia using full-waveform tomography: Constraints on India-Asia collisional tectonics: Earth and Planetary Science Letters, v. 639, p. 118764.

McKenzie, D., and Priestley, K., 2016, Speculations on the formation of cratons and cratonic basins: Earth and Planetary Science Letters, v. 435, p. 94-104.

Mitchell, R. H., and Bergman, S. C., 1991, Petrology of lamproites, New York, Plenum Press.

Molnar, P., England, P., and Martinod, J., 1993, Mantle Dynamics, Uplift of the Tibetan Plateau, and the Indian Monsoon: Reviews of Geophysics, v. 31, no. 4, p. 357-396.

Prelević, D., Brügmann, G., Barth, M., Bozovic, M., Cvetkovic, V., Foley, S. F., and Maksimovic, Z., 2015, Os-isotope constraints on the dynamics of orogenic mantle: The case of the Central Balkans: Gondwana Research, v. 27, no. 4, p. 1560-1573.

Rudnick, R. L., and Goldstein, S. L., 1990, The Pb Isotopic Compositions of Lower Crustal Xenoliths and the Evolution of Lower Crustal Pb: Earth and Planetary Science Letters, v. 98, no. 2, p. 192-207.

Spencer, C. J., Mitchell, R. N., and Brown, M., 2021, Enigmatic Mid-Proterozoic Orogens: Hot, Thin, and Low: Geophysical Research Letters, v. 48, no. 16.

Tapponnier, P., Xu, Z. Q., Roger, F., Meyer, B., Arnaud, N., Wittlinger, G., and Yang, J. S., 2001, Oblique stepwise rise and growth of the Tibet plateau: Science, v. 294, no. 5547, p. 1671-1677.

Tilmann, F., Ni, J., Hearn, T., Ma, Y. S., Rapine, R., Kind, R., Mechie, J., Saul, J., Haines, S., Klemperer, S., Brown, L., Pananont, P., Ross, A., Nelson, K. D., Guo, J., Zhao, W., and Team, I. I. S., 2003, Seismic imaging of the downwelling Indian lithosphere beneath central Tibet:

Science, v. 300, no. 5624, p. 1424-1427.

Tommasini, S., Avanzinelli, R., and Conticelli, S., 2011, The Th/La and Sm/La conundrum of the Tethyan realm lamproites: Earth and Planetary Science Letters, v. 301, no. 3-4, p. 469-478.

van Hinsbergen, D. J., 2022, Indian plate paleogeography, subduction and horizontal underthrusting below Tibet: paradoxes, controversies and opportunities: National Science Review, v. 9, no. 8, p. nwac074.

Wang, Q., Hawkesworth, C. J., Wyman, D., Chung, S.-L., Wu, F.-Y., Li, X.-H., Li, Z.-X., Gou, G.-N., Zhang, X.-Z., and Tang, G.-J., 2016, Pliocene-Quaternary crustal melting in central and northern Tibet and insights into crustal flow: Nature Communications, v. 7, no. 1, p. 11888.

Wang, Q., Zhang, P. Z., Freymueller, J. T., Bilham, R., Larson, K. M., Lai, X., You, X. Z., Niu, Z. J., Wu, J. C., Li, Y. X., Liu, J. N., Yang, Z. Q., and Chen, Q. Z., 2001, Present-day crustal deformation in China constrained by global positioning system measurements: Science, v. 294, no. 5542, p. 574-577.

Wang, Y., Foley, S. F., Buhres, S., Soldner, J., and Xu, Y. G., 2021, Origin of potassic postcollisional volcanic rocks in young, shallow, blueschist-rich lithosphere: Science Advances, v. 7, no. 29, p. 1-8.

Xia, B., Artemieva, I. M., Thybo, H., and Klemperer, S. L., 2023, Strong Variability in the Thermal Structure of Tibetan Lithosphere: Journal of Geophysical Research-Solid Earth, v. 128, no. 3, p. 1-23.

Yin, A., and Harrison, T. M., 2000, Geologic Evolution of the Himalayan-Tibetan Orogen: Annual Review of Earth and Planetary Sciences, v. 28, no. 1, p. 211-280.

Zhang, X. Z., Dong, Y. S., Wang, Q., Dan, W., Zhang, C., Deng, M. R., Xu, W., Xia, X. P., Zeng, J. P., and Liang, H., 2016, Carboniferous and Permian evolutionary records for the Paleo-Tethys Ocean constrained by newly discovered Xiangtaohu ophiolites from central Qiangtang, central Tibet: Tectonics, v. 35, no. 7, p. 1670-1686.

Figure 1

Fig. 1

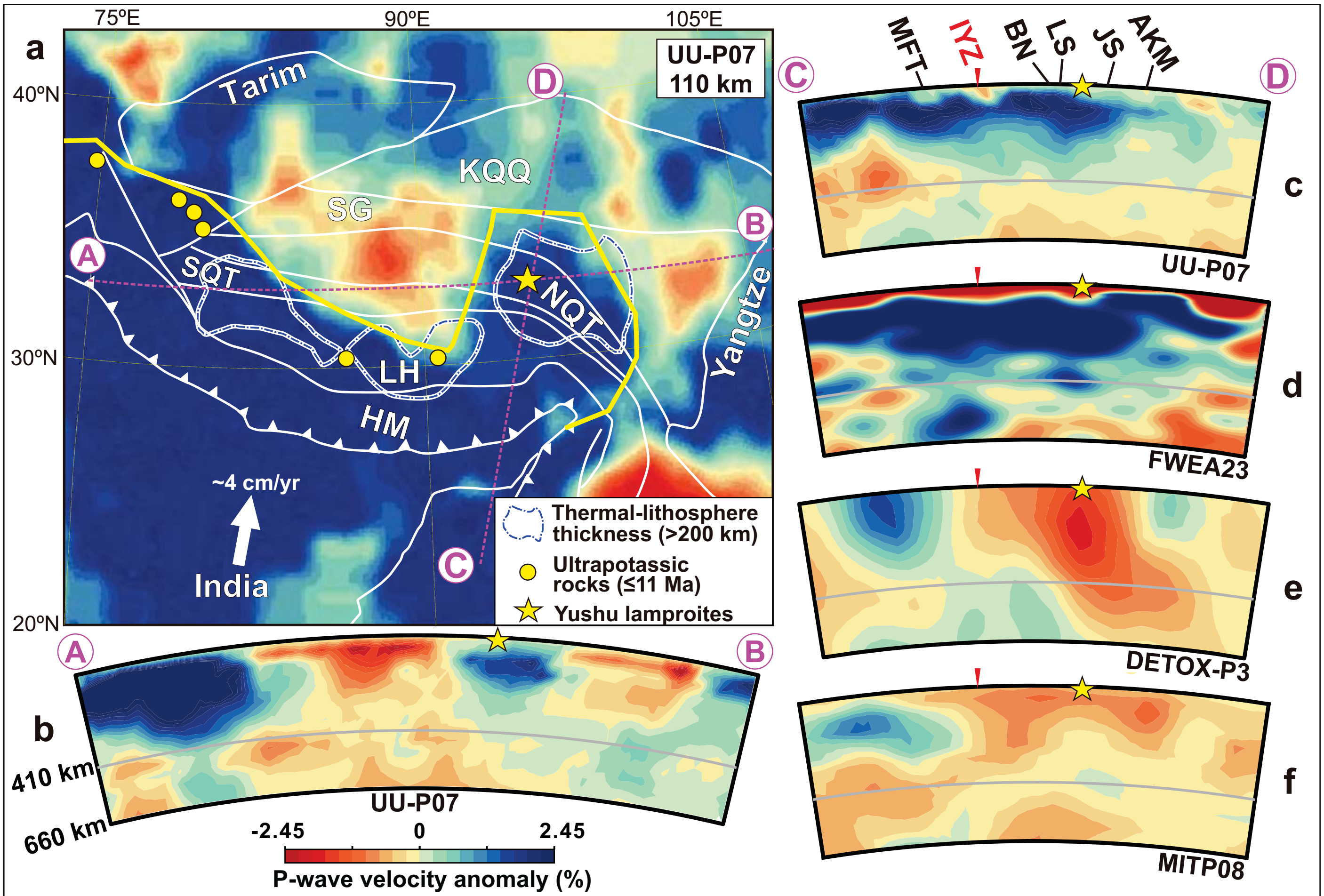

Terrane: HM = Himalaya; **KQQ** = Kunlun–Qaidam–Qilian; **LH** = Lhasa; **NQT** = Northern Qiangtang; **SG** = Songpan–Ganzi; **SQT** = Southern Qiangtang

Suture: AKM = Anyimaqen–Kunlun–Mutztagh; **BN** = Bangong–Nujiang; **IYZ** = Indus–Yarlung Zangbo; **JS** = Jinshajiang; **LS** = Longmuco–Shuanghu; **MFT** = Main Frontal Thrust

Figure 2

Fig. 2

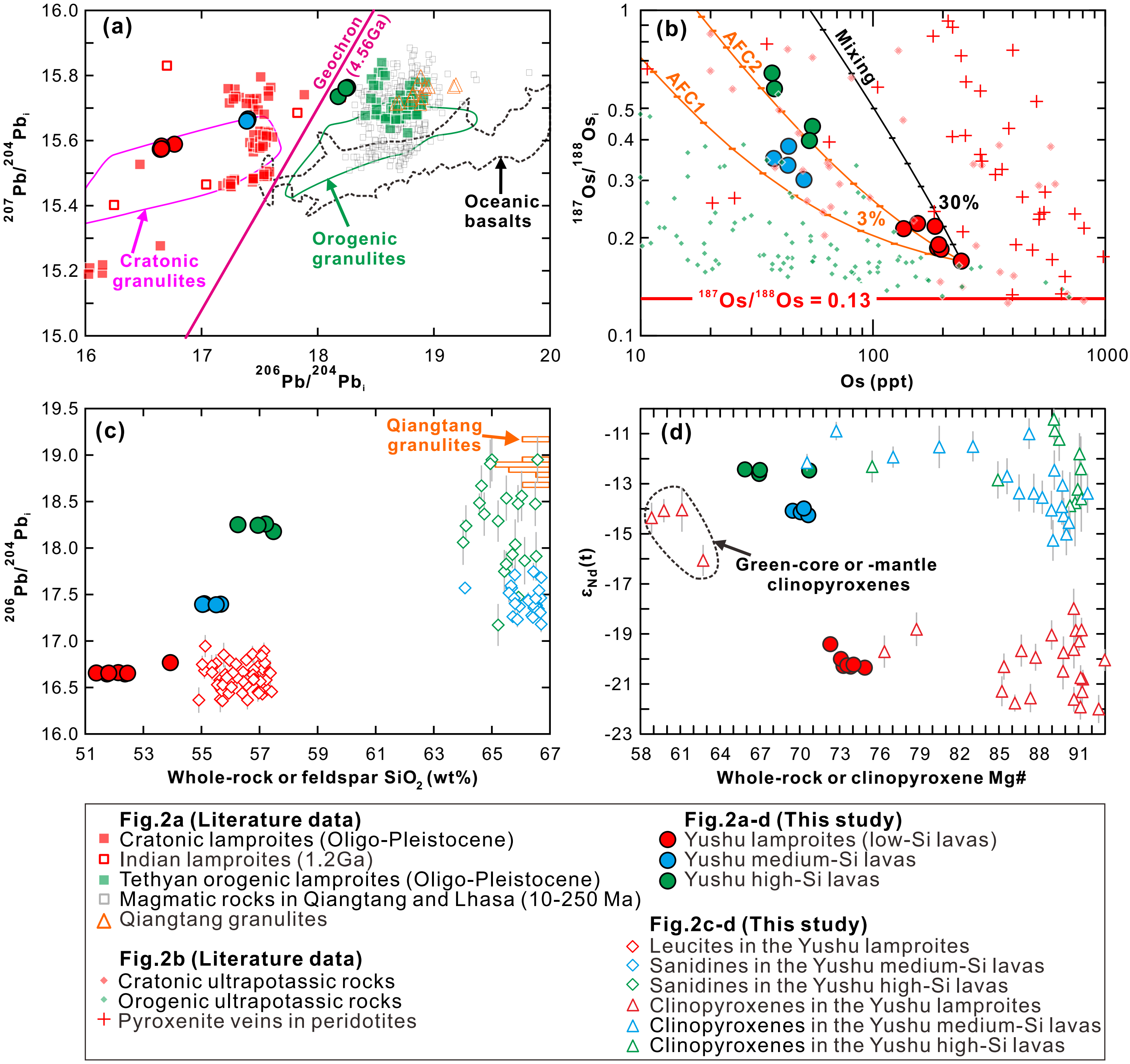

Fig. 3

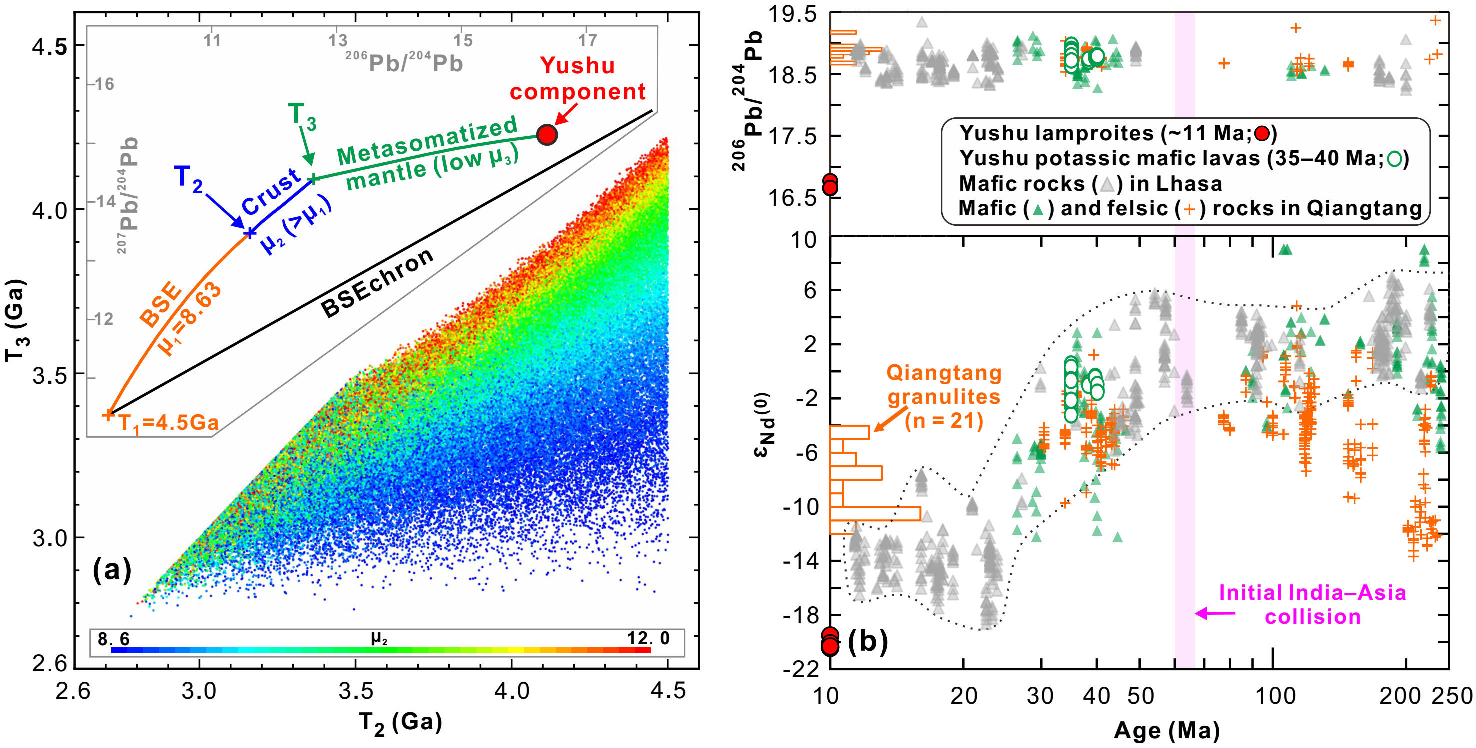

(a)
T1=4.5Ga
BSE
μ1=8.63
T2
Crust
μ2 (>μ1)
T3
Metasomatized mantle (low μ3)
Yushu component
BSEchron
206Pb/204Pb
207Pb/204Pb
μ2
8.6
12.0
T2 (Ga)
T3 (Ga)
(b)
Yushu lamproites (~11 Ma;)
Yushu potassic mafic lavas (35–40 Ma;)
Mafic rocks ( ) in Lhasa
Mafic ( ) and felsic ( ) rocks in Qiangtang
Qiangtang granulites (n = 21)
Initial India–Asia collision
206Pb/204Pb
εNd(0)
Age (Ma)

Figure 4

Fig. 4